

Impermeable Atomic Membranes from Graphene Sheets

J. Scott Bunch, Scott S. Verbridge, Jonathan S. Alden, Arend M. van der Zande, Jeevak M. Parpia, Harold G. Craighead, and Paul L. McEuen*

Cornell Center for Materials Research, Cornell University, Ithaca, New York 14853

Received May 21, 2008; Revised Manuscript Received June 12, 2008

ABSTRACT

We demonstrate that a monolayer graphene membrane is impermeable to standard gases including helium. By applying a pressure difference across the membrane, we measure both the elastic constants and the mass of a single layer of graphene. This pressurized graphene membrane is the world's thinnest balloon and provides a unique separation barrier between 2 distinct regions that is only one atom thick.

Membranes are fundamental components of a wide variety of physical, chemical, and biological systems, used in everything from cellular compartmentalization to mechanical pressure sensing. They divide space into two regions, each capable of possessing different physical or chemical properties. A simple example is the stretched surface of a balloon, where a pressure difference across the balloon is balanced by the surface tension in the membrane. Graphene, a single layer of graphite, is the ultimate limit: a chemically stable and electrically conducting membrane one atom in thickness.^{1–3} An interesting question is whether such an atomic membrane can be impermeable to atoms, molecules and ions. In this letter, we address this question for gases. We show that these membranes are impermeable and can support pressure differences larger than one atmosphere. We use such pressure differences to tune the mechanical resonance frequency by ~ 100 MHz. This allows us to measure the mass and elastic constants of graphene membranes. We demonstrate that atomic layers of graphene have stiffness similar to bulk graphite ($E \sim 1$ TPa). These results show that single atomic sheets can be integrated with microfabricated structures to create a new class of atomic scale membrane-based devices.

A schematic of the device geometry used here—a graphene-sealed microchamber—is shown in Figure 1a. Graphene sheets are suspended over predefined wells in silicon oxide using mechanical exfoliation (see Supporting Information). Each graphene membrane is clamped on all sides by the van der Waals force between the graphene and SiO₂, creating a $\sim(\mu\text{m})^3$ volume of confined gas. The inset of Figure 1a shows an optical image of a single layer graphene sheet forming a sealed square drumhead with a width $W = 4.75 \mu\text{m}$ on each side. Raman spectroscopy was

used to confirm that this graphene sheet was a single layer in thickness.^{4–6} Chambers with graphene thickness from 1 to ~ 75 layers were studied.

After initial fabrication, the pressure inside the microchamber, p_{int} , is atmospheric pressure (101 kPa). If the pressure external to the chamber, p_{ext} , is changed, we found that p_{int} will equilibrate to p_{ext} on a time scale that ranges from minutes to days, depending on the gas species and the temperature. On shorter time scales than this equilibration time, a significant pressure difference $\Delta p = p_{\text{int}} - p_{\text{ext}}$ can exist across the membrane, causing it to stretch like the surface of a balloon (Figure 1b). Examples are shown for $\Delta p > 0$ in Figure 1c and $\Delta p < 0$ in Figure 1d.

To create a positive pressure difference, $\Delta p > 0$, as shown in Figure 1c, we place a sample in a pressure chamber with $p_{\text{ext}} = 690$ kPa N₂ gas for 3 h. After it is removed, a tapping mode atomic force microscope (AFM) image at ambient external pressure (Figure 1c) shows that the membrane bulges upward. Similarly, we can create a lower pressure in the chamber, $\Delta p < 0$, by storing the device under vacuum and then returning it to atmospheric pressure. The graphene-sealed microchamber from Figure 1a (inset) is placed in a pressure of ~ 0.1 Pa for 4 days and then imaged in ambient conditions by AFM (Figure 1d). The graphene membrane is now deflected downward indicating $p_{\text{int}} < p_{\text{ext}}$.

Over time, the internal and external pressures equilibrate. Figure 1e shows a series of AFM line traces through the center of the graphene membrane taken over a period of 3 days. The deflection z at the center of the membrane is initially $z_0 = 175$ nm and decreases slowly over time, indicating a slow air leak from the microchamber. The time scale for decay is approximately 24 h. We characterize the

* Corresponding author. E-mail: mceuen@ccmr.cornell.edu.

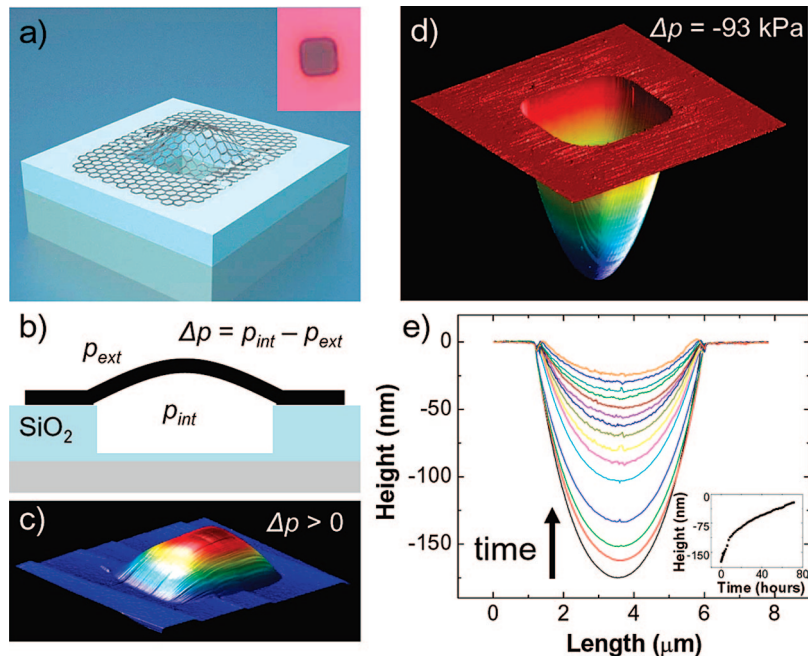


Figure 1. (a) Schematic of a graphene sealed microchamber. (Inset) optical image of a single atomic layer graphene drumhead on 440 nm of SiO₂. The dimensions of the microchamber are 4.75 μm × 4.75 μm × 380 nm. (b) Side view schematic of the graphene sealed microchamber. (c) Tapping mode atomic force microscope (AFM) image of a ~9 nm thick many layer graphene drumhead with Δp > 0. The dimensions of the square microchamber are 4.75 μm × 4.75 μm. The upward deflection at the center of the membrane is z = 90 nm. (d) AFM image of the graphene sealed microchamber of Figure 1a with Δp = -93 kPa across it. The minimum dip in the z direction is 175 nm. (e) AFM line traces taken through the center of the graphene membrane of (a). The images were taken continuously over a span of 71.3 h and in ambient conditions. (Inset) deflection at the center of the graphene membrane vs time. The first deflection measurement (z = 175 nm) is taken 40 min after removing the microchamber from vacuum.

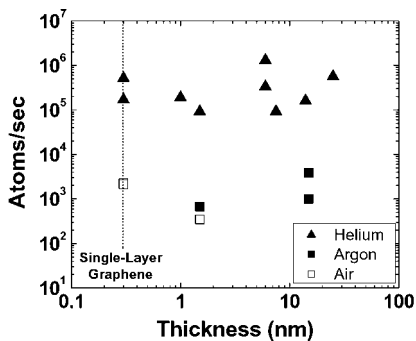


Figure 2. Scatter plot of the gas leak rates vs thickness for all the devices measured. Helium rates are shown as solid triangles (▲), argon rates are shown as solid squares (■) and air rates are shown as hollow squares (□).

equilibration process by monitoring the pressure change and using the ideal gas law to convert this to a leak rate:

$$\frac{dN}{dt} = \frac{V}{k_B T} \frac{dp_{in}}{dt} \quad (1)$$

where N is the number of atoms or molecules in the chamber (see Supporting Information). Figure 2 shows results for several different membranes of various thicknesses and for different gases. Air and argon show similar leak rates, and helium is 2 orders of magnitude faster. The helium leak rates ranged from 10⁵ to ~10⁶ atoms/s with no noticeable dependence on thickness from 1 to 75 atomic layers. All the data were taken in a similar manner where approximately the same pressure difference was applied across the membrane (see Supporting Information and Figure S2).

The lack of dependence of the leak rate on the membrane thickness indicates that the leak is not through the graphene sheets, or through defects in these sheets. This suggests it is either through the glass walls of the microchamber or through the graphene-SiO₂ sealed interface. The former can be estimated from the known properties of He diffusion through glass.⁷ Using Fick's law of diffusion and typical dimensions for our microchambers, we estimate a rate of ~ (1–5) × 10⁶ atoms/s. This is close to the range of values measured (Figure 2).

Using this measured leak rate, we estimate an upper bound for the average transmission probability of a He atom impinging on a graphene surface as

$$\frac{dN}{dt} \frac{2d}{Nv} < 10^{-11} \quad (2)$$

where dN/dt is the measured leak rate, d is the depth of the microchamber, and v is the velocity of He atoms (see Supporting Information). In all likelihood, the true permeability is orders of magnitude lower than the bound given above. Simple estimates based on WKB tunneling of He atoms through a perfect graphene barrier (~8.7 eV barrier height, 0.3 nm thickness) and through a “window” mechanism whereby temporary bond breaking lowers the barrier height to ~3.5 eV, give a tunneling probability at room temperature many orders of magnitude smaller than we observe^{8–10} (see Supporting Information). If we approximate helium atoms as point particles, classical effusion through single atom lattice vacancies in the graphene membrane occurs in ~1 s and therefore much faster than the rates we measure (see Supporting Information). We therefore conclude

that the graphene layer is essentially perfect and for all intents and purposes impermeable to all standard gases, including He.

The impermeability of the graphene membrane allows us to use pressure differences to apply a large, well-defined force that is uniformly distributed across the entire surface of the membrane. This ability to create controlled strain in the membrane has many uses. First, we can measure the elastic properties of the graphene sheet. A well-known and reliable method used to study the elastic properties of films is the bulge test technique.¹¹ The deflection of a thin film is measured as a uniform pressure is applied across it. This surface tension, S , is the sum of two components: $S = S_0 + S_p$ where S_0 is the initial tension per unit length along the boundary and S_p is the pressure-induced tension. Tension is directly related to the strain, ϵ , as $S = Et/(1 - \nu)\epsilon$, where E is the Young's modulus, t is the thickness, and ν is Poisson's ratio. For the geometry of a square membrane, the pressure difference as a function of deflection can be expressed as¹¹

$$\Delta p = \frac{4z}{W^2} \left(c_1 S_0 + \frac{4c_2 Etz^2}{W^2(1 - \nu)} \right) \quad (3)$$

where $c_1 = 3.393$ and $c_2 = (0.8 + 0.062\nu)^{-3}$.

Using the deflection and pressure difference in Figure 1d and accounting for initial slack in the membrane as discussed later in the text, we determine the elastic constants of graphene to be $Et/(1 - \nu) = 390 \pm 20$ N/m (see Supporting Information). The accepted values for the experimental and theoretical elastic constants of bulk graphite and graphene—both 400 N/m^{12–14}—are within the experimental error of our measurement. This is an important result in nanomechanics considering the vast literature examining the relevance of using elastic constants for bulk materials to describe atomic scale structures.^{12,15}

The surface tension in the pressurized membrane can be readily obtained from the Young–Laplace equation, $\Delta p = S(1/R_x + 1/R_y)$ where $R_{x(y)}$ is the radius of curvature of the surface along the $x(y)$ direction. The shape of the bulged membrane with $\Delta p = -93$ kPa in Figure 1d directly gives $R_{x(y)}$. At the point of maximum deflection, we measure this radius of curvature by AFM to be $R_x = R_y = 21$ μm , which amounts to a surface tension $S = 1$ N/m. This is 14 times the surface tension of water but corresponds to a small strain in the graphene of 0.26%. The atomically thin sealed chambers reported here can support pressures up to a few atmospheres. Beyond this, we observe that the graphene slips on the surface. Improved clamping could increase allowable pressure differentials dramatically.

This pressure induced strain in the membrane can also be used to control the resonance frequency of the suspended graphene. This is shown in Figure 3a for a monolayer device prepared with a small gas pressure p_{int} in the chamber. Figure 3b shows results on a 1.5 nm thick membrane. The vibrations of the membrane are actuated and measured optically, as previously reported.² The frequency changes dramatically with external pressure, exhibiting a sharp minimum at a specific pressure and growing on either side. Sufficiently far

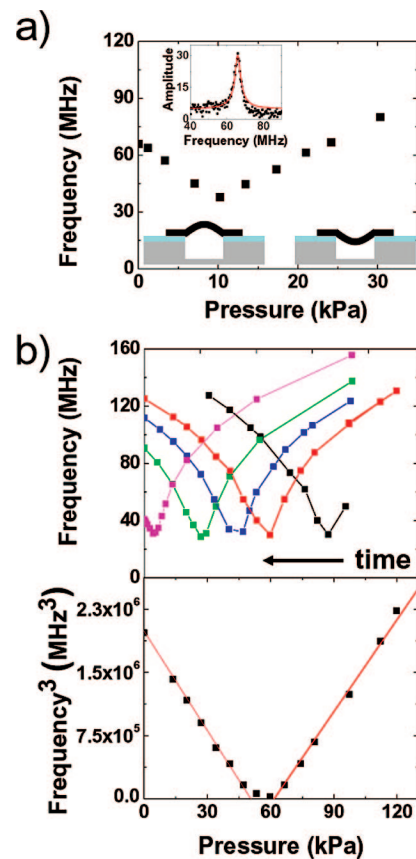


Figure 3. (a) Resonance frequency vs external pressure for the single-layer graphene sealed microchamber shown in Figure 1a. (Upper inset) resonance frequency curve taken at $p_{\text{ext}} = 27$ Pa with a resonance frequency of $f = 66$ MHz and $Q = 25$. (Lower insets) schematic of the configuration of the microchamber at various applied pressures. The graphene is puffed upward or downward depending on Δp . (b) (Upper) resonance frequency vs p_{ext} for a 1.5 nm thick few layer graphene sealed microchamber. Each curve was taken at a different time over a span of 207 h, and the device was left in $p_{\text{ext}} \sim 0.1$ mPa in between each measurement. (Lower) (resonance frequency)³ vs p_{ext} for the red scan in Figure 4b. A linear fit to the data is shown in red.

from the minimum frequency, f_0 , the frequency scales as $f^3 \propto \Delta p$ (Figure 3b).

This behavior follows from the pressure induced changes in the tension S in the membrane. Neglecting the bending rigidity gives the fundamental frequency of a square membrane under uniform tension as

$$f = \sqrt{\frac{S_0 + S_p}{2mW^2}} \quad (4)$$

where m is the mass per unit area.¹⁶ Sufficiently far from f_0 , eqs 3 and 4 can be combined with the approximation, $S \approx \Delta p W^2/16z$ to get the following expression:

$$f^3 = \Delta p \sqrt{\frac{c_2 Et}{2048m^3 W^4(1 - \nu)}} \quad (5)$$

This gives the functional form observed in Figure 3b with the prefactor consisting of the elastic constants of the membrane and the mass. Using $Et/(1 - \nu)$ determined previously, we fit (5) to the data of Figure 3a and 3b to determine the mass per area of the membranes. We find m

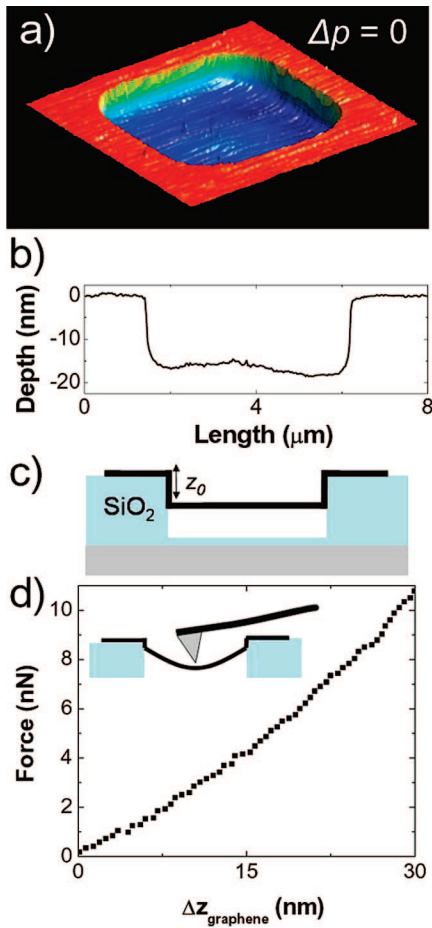


Figure 4. (a) Tapping mode AFM image of the single-layer graphene sealed microchamber shown in Figure 1a with $\Delta p = 0$. (b) Line cut through the center of the graphene membrane in (a). (c) Schematic of the graphene membrane at $\Delta p = 0$ with an initial deflection z_0 due to self-tensioning. (d) Force–distance curve taken at the center of the graphene membrane in (a) at $\Delta p = 0$. The spring constant of the cantilever used is $k_{\text{tip}} = 0.67$ N/m.

$= (9.6 \pm 0.6) \times 10^{-7}$ kg/m² for the monolayer of Figure 3a. This is 30% higher than the theoretical value for a single layer of graphene of 7.4×10^{-7} kg/m². One possibility for this extra mass is adsorbates which would significantly shift the mass of a single atom membrane. The 1.5 nm thick few-layer membrane of Figure 3b has a $m = (3.1 \pm 0.2) \times 10^{-6}$ kg/m². This corresponds to ~ 4 atomic layers in thickness. Previous attempts to deduce the mass from resonance measurements of doubly clamped beams were obscured by the large initial tension in the resonators.² Exploiting the impermeability of graphene membranes to controllably tune the resonance frequency gives us the mass of the suspended graphene membrane regardless of this initial tension. To our knowledge, this is the first direct measurement of the mass of graphene. This ability to measure the mass of the suspended graphene can be used to count the number of layers for multilayered sheets as well as to weigh any adsorbates.

The minimum frequency, f_0 , corresponds to $S_p = 0$, i.e., $p_{\text{int}} = p_{\text{ext}}$. The monolayer graphene membrane in Figure 3a has $f_0 = 38$ MHz when $\Delta p = 0$. This frequency is significantly higher than expected for a graphene square plate under zero tension (0.3 MHz) suggesting that at $\Delta p = 0$, the resonance frequency is dominated by S_0 and not the

bending rigidity. Using the experimentally measured mass of the monolayer membrane above, we deduce an $S_0 \sim 0.06$ N/m. This is similar to what was previously observed in doubly clamped graphene beams fabricated by the same method.²

The origin of this tension is clear from Figure 4a, which shows a tapping-mode AFM image of the suspended monolayer graphene membrane of Figure 1d with $\Delta p = 0$. The image shows the graphene membrane to have a ~ 17 nm dip along the edges of the suspended regions where the graphene meets the SiO₂ sidewalls (Figure 4b). This results from the strong van der Waals interaction between the edge of the graphene membrane and the SiO₂ sidewalls (Figure 4c), which previously has been estimated to be $U \sim 0.1$ J/m².^{17,18} This attraction yields a surface tension $S_0 = U \sim 0.1$ N/m, which is close to the value extracted from the resonance measurement.

The tension in the membrane can also be probed by pushing on the membrane with a calibrated AFM tip.¹⁹ This force-deflection curve gives a direct measure of the spring constant $k_{\text{graphene}} = 0.2$ N/m of the graphene membrane, as shown in Figure 4d. Neglecting the bending rigidity, the tension can be obtained using $S \approx (k_{\text{graphene}}/2\pi) \ln(R/r)$, where R is the radius of the membrane and r is the radius of the AFM tip.²⁰ Assuming $r \sim 50$ nm gives $S \sim 0.1$ N/m, close to both the theoretical value and the value measured using the resonance frequency technique above. These results show that self-tensioning in these thin graphene sheets dominates over the bending rigidity, and this tension will smooth corrugations that may occur in tension-free graphene membranes.³

We envision many applications for these graphene sealed microchambers. They can act as compliant membrane sensors that probe pressures in small volumes and explore pressure changes associated with chemical reactions, phase transitions, and photon detection.^{21,22} In addition to these spectroscopic studies, graphene drumheads offer the opportunity to probe the permeability of gases through atomic vacancies in single layers of atoms²³ and defects patterned in the graphene membrane can act as selective barriers for ultrafiltration.^{24,25} The tensioned suspended graphene membranes also provide a platform for STM imaging of both graphene^{26–28} and graphene–fluid interfaces and offer a unique separation barrier between two distinct phases of matter that is only one atom thick.

Acknowledgment. This work was supported by the NSF through the Cornell Center for Materials Research and Center for Nanoscale Systems and, and by the MARCO Focused Research Center on Materials, Structures, and Devices. Sample fabrication was performed at the Cornell node of the National Nanofabrication Users Network, funded by NSF. We thank Lihong Herman, Jiwoong Park, and Michael Jaquith for help with the spring constant calibration of the AFM tip. We also thank Alan Zehnder for useful discussion

Supporting Information Available: Experimental Methods, Slack and Self Tensioning at $\Delta p = 0$, Measuring the Gas Leak Rates, Transmission Probability, Tunneling of

Helium Atoms across a Graphene Sheet, and Classical Effusion through Single Atom Lattice Vacancies. This material is available free of charge via the Internet at <http://pubs.acs.org>.

References

- (1) Geim, A. K.; Novoselov, K. S. *Nat. Mater.* **2007**, *6* (3), 183–191.
- (2) Bunch, J. S.; van der Zande, A. M.; Verbridge, S. S.; Frank, I. W.; Tanenbaum, D. M.; Parpia, J. M.; Craighead, H. G.; McEuen, P. L. *Science* **2007**, *315* (5811), 490–493.
- (3) Meyer, J. C.; Geim, A. K.; Katsnelson, M. I.; Novoselov, K. S.; Booth, T. J.; Roth, S. *Nature* **2007**, *446* (7131), 60–63.
- (4) Graf, D.; Molitor, F.; Ensslin, K.; Stampfer, C.; Jungen, A.; Hierold, C.; Wirtz, L. *Nano Lett.* **2007**, *7* (2), 238–242.
- (5) Ferrari, A. C.; Meyer, J. C.; Scardaci, V.; Casiraghi, C.; Lazzeri, M.; Mauri, F.; Piscanec, S.; Jiang, D.; Novoselov, K. S.; Roth, S.; Geim, A. K. *Phys. Rev. Lett.* **2006**, *97* (18), 187401.
- (6) Gupta, A.; Chen, G.; Joshi, P.; Tadigadapa, S.; Eklund, P. C. *Nano Lett.* **2006**.
- (7) Perkins, W. G.; Begeal, D. R. *J. Chem. Phys.* **1971**, *54* (4), 1683–1694.
- (8) Saunders, M.; Jimenez-Vazquez, H. A.; Cross, R. J.; Poreda, R. J. *Science* **1993**, *259* (5100), 1428–1430.
- (9) Murry, R. L.; Scuseria, G. E. *Science* **1994**, *263* (5148), 791–793.
- (10) Hrusak, J.; Bohme, D. K.; Weiske, T.; Schwarz, H. *Chem. Phys. Lett.* **1992**, *193* (1–3), 97–100.
- (11) Vlassak, J. J.; Nix, W. D. *J. Mater. Res.* **1992**, *7* (12), 3242–3249.
- (12) Huang, Y.; Wu, J.; Hwang, K. C. *Phys. Rev. B* **2006**, *74* (24), 245413–9.
- (13) Blakslee, O. L.; Proctor, D. G.; Seldin, E. J.; Spence, G. B.; Weng, T. *J. Appl. Phys.* **1970**, *41* (8), 3373–3382.
- (14) Kelly, B. T. *Physics of graphite. Applied Science*; Prentice Hall: London, Englewood, NJ, 1981; p 477.
- (15) Yakobson, B. I.; Brabec, C. J.; Bernholc, J. *Phys. Rev. Lett.* **1996**, *76* (14), 2511–2514.
- (16) Timoshenko, S.; Young, D. H.; Weaver, W. *Vibration Problems in Engineering*, 4th ed.; John Wiley and Sons, Inc.: New York, 1974; pp 481–484.
- (17) Hertel, T.; Walkup, R. E.; Avouris, P. *Phys. Rev. B* **1998**, *58* (20), 13870–13873.
- (18) Ruoff, R. S.; Tersoff, J.; Lorents, D. C.; Subramoney, S.; Chan, B. *Nature* **1993**, *364* (6437), 514–516.
- (19) Frank, I. W.; Tanenbaum, D. M.; van der Zande, A. M.; McEuen, P. L. *J. Vac. Sci. Technol., B* **2007**, *25* (6), 2558–2561.
- (20) Tanizawa, K.; Yamamoto, K. *National Committee for Theoretical and Applied Mechanics, Science Council of Japan* **2004**, *53*, 75–82.
- (21) Jiang, C.; Markutsya, S.; Pikus, Y.; Tsukruk, V. V. *Nat. Mater.* **2004**, *3* (10), 721–728.
- (22) Mueggenburg, K. E.; Lin, X.-M.; Goldsmith, R. H.; Jaeger, H. M. *Nat. Mater.* **2007**, *6* (9), 656–660.
- (23) Hashimoto, A.; Suenaga, K.; Gloter, A.; Urita, K.; Iijima, S. *Nature* **2004**, *430* (7002), 870–873.
- (24) Rose, F.; Debray, A.; Martin, P.; Fujita, H.; Kawakatsu, H. *Nanotechnology* **2006**, (20), 5192.
- (25) Striemer, C. C.; Gaborski, T. R.; McGrath, J. L.; Fauchet, P. M. *Nature* **2007**, *445* (7129), 749–753.
- (26) Stolyarova, E.; Rim, K. T.; Ryu, S.; Maultzsch, J.; Kim, P.; Brus, L. E.; Heinz, T. F.; Hybertsen, M. S.; Flynn, G. W. *Proc. Natl. Acad. Sci.* **2007**, *104* (22), 9209–9212.
- (27) Ishigami, M.; Chen, J. H.; Cullen, W. G.; Fuhrer, M. S.; Williams, E. D. *Nano Lett.* **2007**, *7* (6), 1643–1648.
- (28) Rutter, G. M.; Crain, J. N.; Guisinger, N. P.; Li, T.; First, P. N.; Stroschio, J. A. *Science* **2007**, *317* (5835), 219–222.

NL801457B